



PERGAMON

Available online at www.sciencedirect.com

SCIENCE @ DIRECT®

Physics and Chemistry of the Earth 28 (2003) 669–679

PHYSICS
and CHEMISTRY
of the EARTH

www.elsevier.com/locate/pce

Towards the identification of siderite, rhodochrosite, and vivianite in sediments by their low-temperature magnetic properties

T. Frederichs^{a,*}, T. von Dobeneck^{a,b}, U. Bleil^a, M.J. Dekkers^b

^a Department of Geosciences, University of Bremen, P.O. Box 330 440, D-28334 Bremen, Germany

^b Paleomagnetic Laboratory Fort Hoofddijk, Utrecht University, Budapestlaan 17, 3584 CD, Utrecht, The Netherlands

Abstract

Siderite (FeCO_3), rhodochrosite (MnCO_3), and vivianite ($[\text{Fe}_3(\text{PO}_4)_2] \cdot 8 \text{H}_2\text{O}$) are well-known authigenic minerals in a number of sedimentary settings. Here, we explore the potential of low-temperature mineral magnetic techniques for their identification at low concentration in bulk samples thus expanding mineral magnetic proxies for environmental purposes. The basic rock magnetic properties of these minerals, which are paramagnetic at ambient temperature, were determined with a 'Magnetic Properties Measurement System'. Well-crystalline chemically analyzed material of natural origin was used to gather these data. The diagnostic value of the observed specific magnetic properties was tested on two mid-Eocene sediment samples from the Norwegian Sea (ODP Leg 104, Site 643) known to contain these minerals.

The observed Néel temperatures of siderite (37 K) and rhodochrosite (34 K) conform with literature data. Both carbonates show a fairly strong spin-canted remanence ($\sim 0.4 \text{ Am}^2/\text{kg}$) from cooling in a 5 T magnetic field. Different ratios of field-cooled and zero-field-cooled remanences, however, allow a discrimination between the two minerals. A characteristic of rhodochrosite is its extremely high magnetic susceptibility just below the Néel temperature. An almost vertical slope in very low fields of the hysteresis loop also testifies to this high susceptibility. It is assigned to a weak anisotropic ferromagnetism confined to the basal plane in which the spontaneous magnetization can almost freely rotate. A prominent magnetic property of siderite is its metamagnetism, resulting in a progressively upward bending of the hysteresis curve in magnetic fields above 5 T. Vivianite also shows an onset of metamagnetic transition below 5 K in 5 T fields and a 'two-stage' increase in susceptibility between 2 and 12 K attributed to successive short- and long-range magnetic ordering. The magnetic properties of the two authigenic marine sediments could be largely explained by combining characteristics of rhodochrosite and manganosiderite. Shifting of the Néel points to lower temperatures and less well pronounced magnetic phenomena are attributed to element substitution and non-stoichiometry which occur commonly in sedimentary environments.

© 2003 Elsevier Ltd. All rights reserved.

Keywords: Siderite; Rhodochrosite; Vivianite; Mineral magnetism; Low-temperature magnetism; Metamagnetism

1. Introduction

In rock and environmental magnetism the magnetic properties of rocks, sediments, and soils are physically investigated to explain their provenance and genesis. Variations in concentration, mineralogy, and grain size serve as proxy parameters in manifold applications, e.g., in paleoclimate or source tracing studies (Frederichs et al., 1999; Maher and Thompson, 1999). In general, these studies refer to minerals that are ferri- or anti-ferromagnetic at room temperature, i.e., to minerals that are able to carry a remanent magnetization under

ambient conditions. These 'magnetic minerals' include iron oxides, sulfides and oxyhydroxides. Their specific properties allow a discrimination and quantification by magnetic bulk sample measurements (Peters, 1995; Peters and Thompson, 1999; Peters and Dekkers, 2003).

In the course of sediment diagenesis, various secondary iron and manganese minerals form which are in most cases paramagnetic at room temperature. Among these authigenic minerals are the iron carbonate siderite (FeCO_3), the manganese carbonate rhodochrosite (MnCO_3), and the hydrated iron phosphate vivianite ($[\text{Fe}_3(\text{PO}_4)_2] \cdot 8 \text{H}_2\text{O}$). They are typical of anoxic environments and indicative for geochemical conditions where ferric iron oxides usually dissolve (Canfield et al., 1992). Rhodochrosite is formed in both anoxic sulfidic and non-sulfidic environments whereas siderite is

* Corresponding author. Tel.: +49-421-218-3989; fax: +49-421-218-7008.

E-mail address: thofred@uni-bremen.de (T. Frederichs).

restricted to anoxic non-sulfidic methanic environments (Glasby and Schultz, 1999 and references therein). Both occur in rapidly accumulating, fine-grained, organic-rich sediments, where CO_2 is produced as a result of oxidation of organic matter, partly by reduction of Mn and Fe oxyhydroxides. Biological mediation plays an important role in these processes (Nealson and Saffarini, 1994; Konhauser, 1998). Vivianite forms in iron-rich sediments within or below the sulfate reduction zone or the methanogenic zone (Burns, 1997; Schulz et al., 1994 and references therein).

Authigenic minerals can form rapidly in sediments of quite variable age in either marine or lacustrine settings. In marine settings, rhodochrosite was reported in 7 ka Baltic Sea sediments (Neumann et al., 2002), in 5 Ma old pelagic sediments from the Galapagos Ridge in the equatorial Pacific (Morad and Al-Aasm, 1997), together with siderite in 25 Ma chalks of the Barbados accretionary prism (Housen et al., 1996), and in Norwegian Sea sediments of about the same age (Chow et al., 2000). Siderite was described in 190 ka carbonate oozes from the deep-sea fan of the Congo River (Haese et al., 1997), above and within the gas hydrate zone in Blake Ridge sediments of 6 Ma of age (Rodriguez et al., 2000) and together with vivianite in 25 ka old Amazon Fan sediments (Burns, 1997).

In lacustrine settings, vivianite is reported more often than in marine settings: in recent organic-rich muds from wells in Portugal (Vriend et al., 1991), in subrecent sediments from Baptiste Lake (Alberta, Canada; Manning et al., 1999), in 5 ka old laminated mud from Lake Barrine (Northeast Australia; Walker and Owen, 1999), and also in the Quaternary sediments of Lake Baikal (Russia; Deike et al., 1997). Rhodochrosite was identified in 10 ka old varved lake sediments in Big Watab Lake (Minnesota, USA; Stevens et al., 2000) and siderite in 20 ka old sediments of Amazonian rainforest lakes (Sifeddine et al., 2001).

Hence, siderite, rhodochrosite, and vivianite occur in a wide variety of sedimentary environments. A superficial examination of their magnetic properties may lead to confusion with low-temperature properties of some of the classical magnetic minerals such as pyrrhotite (Dekkers et al., 1989) or superparamagnetic (titano) magnetite (Worm and Jackson, 1999). Minerals not yet fully investigated like ilmenite (Senftle et al., 1975), ferrihydrite (Zergenyi et al., 2000) and lepidocrocite (Hirt et al., 2002) exhibit changes in magnetic susceptibility or remanence at a comparable low-temperature range. Moreover, siderite and probably also vivianite disintegrate into strongly magnetic magnetite and/or maghemite and weakly magnetic hematite upon heating in air (Ellwood et al., 1986, 1989; Pan et al., 2000), disturbing thermal demagnetization that is routinely applied in paleomagnetic analysis. Oxidation of siderite nodules may result in the acquisition of a chemical re-

manent magnetization (Hus, 1990) complicating paleomagnetic interpretation.

Therefore, the detection of siderite, rhodochrosite, and vivianite is important: it puts meaningful constraints on the geochemical environment and allows to optimize paleomagnetic procedures. X-ray diffraction analysis can detect these minerals down to concentrations of about 1–2 wt.%. The ability to identify them in much lower concentrations by magnetic techniques would significantly add to the potential of environmental magnetism. This could be done, for example, by measuring their Néel temperature (T_N), or, more general, their characteristic magnetic ordering temperatures. Magnetic hardness, hysteresis properties, and differences between zero field cooling (ZFC) and field cooling (FC) behavior provide further diagnostic information. Here, we report on these parameters to overcome the presently existing gap in knowledge of mineral magnetic properties.

2. Basic mineral magnetic properties

Siderite (FeCO_3 , density 3960 kg/m^3 ; Hurlbut, 1971) is a brownish translucent mineral crystallizing in the same hexagonal (rhombohedral) lattice as calcite. Mn and Mg can substitute for Fe defining a complete solid solution series to rhodochrosite and magnesite (MgCO_3). Calcium may be present in small amounts. Siderite is antiferromagnetic with a Néel temperature (T_N) of about 38 K (Jacobs, 1963) derived from magnetization data. Jacobs also discovered that the antiferromagnetic lattice of siderite gradually transforms into a ferromagnetic lattice when exposed to strong magnetic fields of 12–14 T. Contemporaneously, Ozhigin (1963) recognized the strong non-linearity of $M(H)$ of FeCO_3 in fields larger than 10 T being very similar to the behavior of ‘metamagnets’. The term metamagnetism was proposed by H.A. Kramers (Bequerel, 1940) and describes the phenomenon of magnetic phase transition from an antiferromagnetic to ferro- or ferrimagnetic state. This effect is observed for numerous antiferromagnetic alloys and also by iron halogenides such as FeCl_2 , FeBr_2 , and FeI_2 (Stryjewski and Giordani, 1977). The unusually broad and high-coercive metamagnetic transition of siderite was theoretically explained by Dudko et al. (1975). They describe the transition as the result of a continuous change of the antiferromagnetic sub-lattice magnetization being oppositely oriented to the external magnetic field and introduce a concept of multi-sub-lattices and successive flipping of individual spins forming a periodic structure in an external magnetic field of 15–18 T.

Rhodochrosite (MnCO_3 , density 3690 kg/m^3 ; Hurlbut, 1971) is a rose-red, transparent to translucent mineral with the same hexagonal symmetry as siderite.

Ca substitution for Mn creates a partial solid solution series with calcite. Mg and Zn can substitute for Mn in limited amounts as well (Hurlbut, 1971). Rhodochrosite is a canted antiferromagnet with $T_N = 32$ K (Borovik-Romanov, 1959) determined also from magnetization data. The author assigns the additional weak anisotropic ferromagnetism to incompletely aligned spins in the antiferromagnetic order of the basal crystal plane. The spontaneous magnetization does not have a fixed direction, but may rotate almost freely in the basal plane. Robie et al. (1984) reported heat capacity data of two samples of carefully characterized rhodochrosite and siderite showing anomalies at 34.27 and 39.71 K due to antiferromagnetic–paramagnetic transitions.

Vivianite ($[\text{Fe}_3(\text{PO}_4)_2] \cdot 8 \text{H}_2\text{O}$, density 2650 kg/m³; Hurlbut, 1971) is a transparent to translucent monoclinic mineral forming prismatic lamellar flakes. It is colorless in its ideal state, but turns vividly blue to green with partial oxidation of Fe^{2+} to Fe^{3+} . Already in the late fifties, Mays (1957) concluded from nuclear magnetic resonance experiments that iron group phosphates such as vivianite undergo antiferromagnetic or ferrimagnetic transitions above the temperature of liquid helium. Vivianite is an antiferromagnet with a Néel temperature of 12 K (Meijer et al., 1967). Kleinberg (1969) discovered that the magnetic structure of vivianite consists of ferromagnetic (001) planes with consecutive planes antiferromagnetically coupled. Forstat et al. (1965) performed specific-heat measurements on a single crystal of vivianite. They associated two anomalies observed at 9.6 and 12.4 K with paramagnetic to antiferromagnetic transitions. The six iron ions per unit cell are not equivalent giving rise to a two-step antiferromagnetic transition. Meijer et al. (1967) also described the presence of two magnetic systems in vivianite. Their moments are oriented perpendicular to each other in the *ac* plane. The magnetic axes rotate by 38° between ~30 and 4 K. Forsyth et al. (1970) determined the magnetic structure of vivianite from a single crystal neutron study and found an angle of 42° between the spin directions on the two different Fe sublattices. They reported a Néel temperature of 8.84 K. Grodzicki and Amthauer (2000) performed cluster molecular orbital calculations to explain the electronic and magnetic structure of vivianite confirming the differences between the two iron sites.

3. Materials and methods

The monomineralic siderite, rhodochrosite and vivianite samples investigated are well-crystalline natural specimens taken from the mineral collection of the Bremen Geosciences Department. They consist of one or a few mineral fragment(s) of 70–200 mg weight which were chipped off macroscopic crystals of hydrothermal origin. The fingertip sized siderite and vivianite crystals are

translucent and have good idiomorphic shapes. Electron microprobe analysis of the siderite sample revealed small admixtures of Cu, Pb and S in form of chalcopyrite (CuFeS_2) and galena (PbS) inclusions. The rhodochrosite mineral sample (pink) is polycrystalline and shows variable stains. Electron microprobe analysis of a fraction of the sample revealed the presence of Ca and Mg. Element distribution images show zones enriched in Mg or Ca. Total solid concentrations of elements Fe, Mn, Ca, Mg, P, Sr, S, Cu, Ni, and Pb were determined by microwave digestion (MLS Ethos 1600) with hydrofluoric acid (Zabel et al., 2001). Subsequent analysis of the digestion solution were made using inductively coupled plasma-optical emission spectrometry (ICP-OES; Perkin Elmer, Optima 3000). Values are listed in Table 1.

The marine sediment samples investigated originate from the Norwegian Sea (ODP Leg 104, Site 643, Sample 44-04-124, 415.78 m core depth and Sample 47-06-28, 446.88 m core depth) and were intensively studied by Henrich (1989). The mid-Eocene hemipelagic clays contain iron and manganese carbonates such as rhodochrosites and transitional rhodochrosite/manganosiderites in significant amounts resulting in sufficiently strong magnetic moments. Also apatite ($\text{Ca}_5[(\text{PO}_4)_3(\text{OH},\text{F},\text{Cl})]$) is present. The authigenic carbonates of the upper sediment sample (44-04-124) are described as rhodochrosite of diffuse large rhombs. The sediment contains 1.6 wt.% Fe and 20.5 wt.% Mn. Mg, Sr and P amounts are well below 1 wt.%. The main component is CaCO_3 with 58.5 wt.%. The lower sediment sample (47-06-28) contains 7.5 wt.% Fe, 18.3 wt.% Mn, 54.7 wt.% CaCO_3 and less than 1 wt.% Mg and P. Henrich (1989) concluded that the rhodochrosites and transitional rhodochrosite/manganosiderites had precipitated at the transition of the sulfate reduction and methane generation zones.

A Quantum Design XL-7 Magnetic Properties Measurement System (MPMS) available at the paleo- and rock magnetic laboratory of the Department of Geosciences of the University of Bremen allowed to perform highly sensitive low-temperature measurements to analyze these authigenic minerals in variable magnetic fields up to 7 T and temperatures from 400 K down to 1.8 K. The crystal chips were randomly oriented in gelatin capsules and stabilized with pure vacuum grease hardening at sub-zero temperatures. All mineral samples gave strong magnetic signals well above the instrumental noise level ($\sim 10^{-11} \text{ Am}^2$).

Most measurements presented follow standardized field–temperature runs commonly applied in low-temperature rock magnetism. Remanent magnetization σ_r was always measured during warming in order to determine the thermal demagnetization of low-temperature remanence. Initially, each sample was cooled in zero field to a temperature of 2 K at which an isothermal remanence was imparted by a direct field of 5 T (ZFC). The superconducting magnet was then quenched to zero

Table 1
Element concentrations of natural siderite, rhodochrosite and vivianite well-crystalline samples determined by ICP-OES

Element	Concentration [mg/l]	SD [%]	Solid phase [g/kg]	Solid phase [mol/kg]
<i>Siderite</i>				
Fe	385	0.18	376	6.73
Mn	28.8	0.28	28.1	0.51
Ca	4.1	0.31	4.0	0.10
Mg	24.2	0.25	23.6	0.97
P	–	–	–	–
Sr	–	–	–	–
S	0.16	4.3	0.16	0.0049
Cu	–	–	–	–
Ni	–	–	–	–
Pb	–	–	–	–
<i>Rhodochrosite^a</i>				
Fe	5.1	0.37	5.0	0.09
Mn	320	1.93	313.7	5.71
Ca	11.7	0.39	11.5	0.29
Mg	6.1	0.29	6.0	0.25
P	0.44	4.31	0.43	0.014
Sr	–	–	–	–
S	1.26	0.82	1.24	0.039
Cu	–	–	–	–
Ni	–	–	–	–
Pb	–	–	–	–
<i>Vivianite</i>				
Fe	304	0.14	299	5.35
Mn	0.16	0.24	0.16	0.0029
Ca	0.07	0.99	0.07	0.0017
Mg	0.16	0.76	0.16	0.0065
P	105	0.65	103.1	3.33
Sr	–	–	–	–
S	–	–	–	–
Cu	–	–	–	–
Ni	–	–	–	–
Pb	–	–	–	–

SD: standard deviation of concentration; '–' not detectable. Weighted sample was 51 mg each.

^a A black precipitation of probably PbCl₂ occurred during the preparation procedure. Therefore the digestion solution was filtered before the ICP-OES measurement. Thus Pb was not detected in the filtered solution and the S content is very likely to represent PbS included in the sample.

field and remanence was measured during warming to 300 K at defined temperature steps. In a second run, the samples were cooled in a direct field of 5 T (FC). At 2 K the magnet was set to zero field and remanence was again measured during warming to 300 K (260 K for the sediment samples, sufficient to reduce the remanence to almost zero). Temperature dependent low-field magnetic *ac* susceptibility χ was determined in alternating fields of 0.4 mT at a frequency of 110 Hz to avoid power frequency disturbance. Hysteresis loops $M(B_0)$ were recorded between peak magnetic fields of ± 5 T at several temperatures below 40 K.

4. Results

4.1. Siderite

During warming from 2 K, both ZFC and FC states of the siderite specimen (Fig. 1a) show a steep rema-

nence decay to almost zero at 37 K. This temperature is in perfect agreement with the literature Néel point (38 K; Jacobs, 1963). Note that the FC remanence at 2 K (0.382 Am²/kg) is about eight times higher than the ZFC remanence (0.052 Am²/kg). This large difference is attributed to an additional thermal remanence acquired during cooling in the 5 T field through the sample's Néel temperature. It implies that siderite is far from magnetic saturation in a field of 5 T at 2 K. We measured various low-temperature pTRM curves during cooling from 50 K down to 2 K and switched the magnetizing field on and off in different temperature intervals in order to determine temperature intervals of preferential FC remanence acquisition. These 'cascading runs' show that the extremely hard coercivity encountered at 2 K softens considerably above 20 K. Simultaneously, in-phase magnetic susceptibility increases from 1.47×10^{-6} m³/kg at 2 K to a peak value of 5.24×10^{-6} m³/kg at 37 K and decreases linearly with $1/T$ during further warming (Fig. 1b). The $1/\chi(T)$ curve

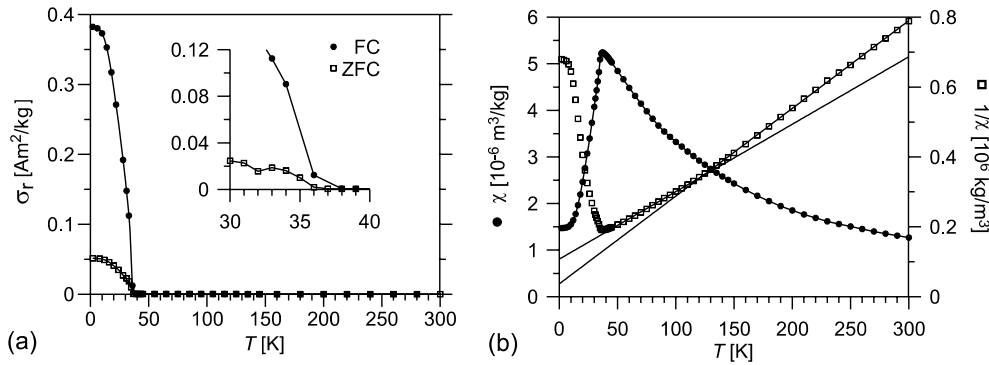


Fig. 1. Low-temperature magnetic characteristics of well-crystalline siderite. (a) Warming curves of a 5 T remanence σ_r after cooling in zero field (open squares) and in a field of 5 T (solid dots). The insert shows the Néel temperature region. For clarity only every second data point is represented by a symbol. (b) In-phase magnetic susceptibility χ versus temperature shows a maximum at the Néel temperature of 37 K. The straight lines mark a fit to the $1/\chi$ curve in the intervals from 50 to 115 K and from 150 to 300 K plotted between the axis limits.

shows a subtle change in slope at around 120 K, possibly related to impurities.

4.2. Rhodochrosite

Warming curves of FC and ZFC remanence for rhodochrosite (Fig. 2a) are similar to those of siderite. Intensities drop significantly at a temperature of 34 K, slightly above the published Néel temperature for rhodochrosite of $T_N = 32$ K (Borovik-Romanov, 1959). FC remanence is only about 40% above the ZFC remanence (0.463 and 0.327 Am²/kg, respectively). This indicates a comparatively higher saturation and therefore more efficient magnetization at 2 K than for siderite, implying a magnetically softer mineral. The 2 K in-phase magnetic susceptibility (Fig. 2b) doubles during warming to 151×10^{-6} m³/kg at 29 K and, unlike for siderite, drops by almost two orders of magnitude to 5.06×10^{-6} m³/kg at 34 K. The 30 times higher susceptibility of rhodochrosite is a consequence of the afore mentioned low anisotropy barriers in its basal plane. Upon warming

above the Néel temperature, inverse susceptibility increases linearly with rising T .

4.3. Vivianite

ZFC and FC warming curves of vivianite (Fig. 3a) are nearly identical, pointing to a magnetically soft mineral saturating in a 5 T field at 2 K. The initial value of FC σ_r (1.94×10^{-3} Am²/kg) decreases sharply to a local minimum at 7.5 K (1.06×10^{-3} Am²/kg), then increases to a local maximum (1.16×10^{-3} Am²/kg) at 12 K and decreases smoothly thereafter without reaching zero. It appears that the magnetization above the Néel point represents an induced paramagnetism of a small residual field of the MPMS instrument. It is visible in case of vivianite, because its remanence is three orders of magnitude smaller than that of siderite and rhodochrosite. The in-phase magnetic susceptibility of vivianite (Fig. 3b) largely resembles the corresponding curve for siderite, both in shape and in amplitude with the exception that the maximum (6.62×10^{-6} m³/kg is

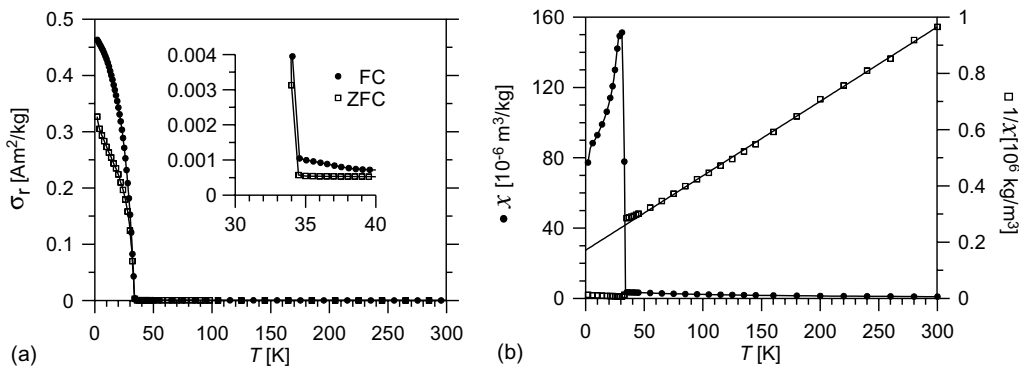


Fig. 2. Low-temperature magnetic characteristics of well-crystalline rhodochrosite. (a) Warming curves of 5 T remanence σ_r after cooling in zero field (open squares) and in a field of 5 T (solid dots). The insert illustrates the steep decay at the Néel temperature and some residual remanence above. For clarity only every fourth data point is represented by a symbol. (b) In-phase magnetic susceptibility χ versus temperature shows a Hopkinson peak below the Néel temperature of 34 K. The straight line marks a fit to the $1/\chi$ curve in the interval from 50 to 300 K plotted between the axis limits.

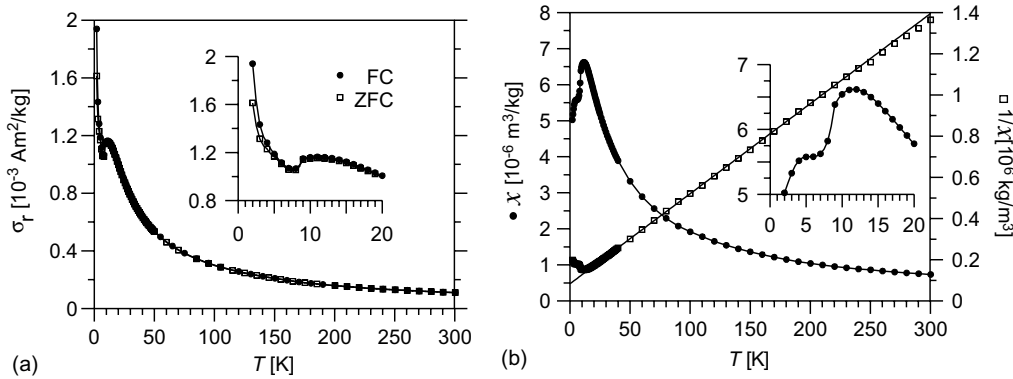


Fig. 3. Low-temperature magnetic characteristics of well-crystalline vivianite. (a) Warming curves of 5 T remanence σ_r after cooling in zero field (open squares) and in a field of 5 T (solid dots). The insert clarifies double kinks at two ordering temperatures and considerable residual remanence above T_N . For clarity only every fourth data point is represented by a symbol. (b) In-phase magnetic susceptibility χ versus temperature shows a maximum at the Néel temperature of 12 K. The straight line marks a fit to the $1/\chi$ curve in the interval from 20 to 300 K plotted between the axis limits. The insert illustrates the ‘two-step’ increase in susceptibility at low temperatures.

located at the Néel temperature of 12 K. An additional feature of the low-temperature branch is a shoulder at 7.5 K.

All observed features are nicely explained by the results of Meijer et al. (1967). They described different magnetic ordering processes as a function of temperature: a ‘quasi two-dimensional ordering’ in the ac planes at 12.4 K, followed by an ordering between the layers at 9.6 K and a third three dimensional long range ordering at 8.85 K. Grodzicki and Amthauer (2000) assign the higher Néel temperature of 12.4 K to antiferromagnetic ordering within chains of alternating A and B octahedra oriented along diagonals of the crystallographic ac plane and linked via phosphate tetrahedra containing the bridging oxygens of the B octahedra. The lower Néel temperature of 9.6 K is attributed to ordering between the chains by fairly strong ferromagnetic interaction between Fe^A and Fe^B spins via the axially coordinated phosphate tetrahedra. Alternatively, the higher Néel temperature might indicate a short-range spin ordering, while the lower T_N corresponds to the onset of long-range two-dimensional ordering. Dekkers et al. (2000) observed a comparable behavior with a local maximum of remanence at ~ 10 K in fresh as well as in stored greigite of various provenances. They speculated on a magnetic transition as a possible explanation for the maximum remanence at ~ 10 K.

4.4. Marine sediment sample 44-04-124

Converting the Mn and Fe concentrations determined by AAS (Henrich, 1989) exclusively into carbonate minerals, this mid-Eocene hemipelagic clay from the Norwegian Sea should contain as much as 42 wt.% $MnCO_3$ and 3 wt.% $FeCO_3$. We therefore expected the sample to show similar magnetic characteristics as the crystalline rhodochrosite. Indeed, the warming curves of

low-temperature remanence (Fig. 4a) basically resemble those of the reference mineral. The difference of the 5 T FC and ZFC remanences at 2 K is only 15%, a strong indication of rhodochrosite (cf. Fig. 2a). It excludes siderite, where this difference is much larger (cf. Fig. 1a). Correcting for absolute concentrations, the 2 K remanence carried by the sedimentary rhodochrosite is twice that of the monomineralic crystalline sample. This could be due to some isomorphous substitution that would influence the spin canting angle or introduce a defect moment, in line with the situation in hematite. FC and ZFC warming curves show a comparably steep and very similar thermal decay reaching the near-zero plateau at only 28 K. Just a small fraction of the FC remanence continues up to 39 K as in the reference sample. It remains an open question, whether the difference of 4 K to the literature Néel temperature of 32 K is due to some Fe substitution or reflects unblocking of remanence. Assuming all iron present is included in rhodochrosite, it implies an about 8% solid solution.

The sediment’s $\chi(T)$ curve (Fig. 4b) shows a spike at 27 K, 2 K lower and much less pronounced than in the reference rhodochrosite (cf. Fig. 2b). This is an indication that the free rotation in the basal plane is hampered by non-stoichiometry. Only just below the Néel point, the energy barrier is passed by thermal activation. The slope of the (inverse) section conforms well with the sedimentary $MnCO_3$ concentration. Furthermore, the susceptibility curve of present paramagnetic minerals indicated by the linearity of the inverse susceptibility (Fig. 4b) above T_N apparently superimpose with $\chi(T)$ for rhodochrosite.

4.5. Marine sediment sample 47-06-28

The second marine sediment sample predominantly consists of rhodochrosites and manganosiderites de-

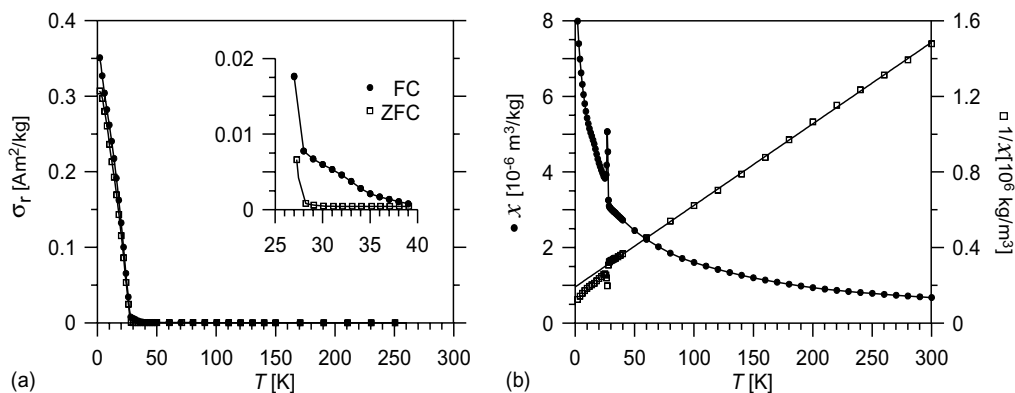


Fig. 4. Low-temperature magnetic characteristics of Norwegian Sea sediment (ODP Site 643, Leg 104, Sample 44-04-124, 415.78 m core depth). (a) Warming curves of 5 T remanence σ_r after cooling in zero field (open squares) and in a field of 5 T (solid dots). The insert clarifies the steep decay of remanence. For clarity only every fourth data point is represented by a symbol. (b) In-phase magnetic susceptibility χ versus temperature shows a Hopkinson peak below the Néel temperature of 29 K. The straight line marks a fit to the $1/\chi$ curve in the interval from 50 to 300 K plotted between axis limits.

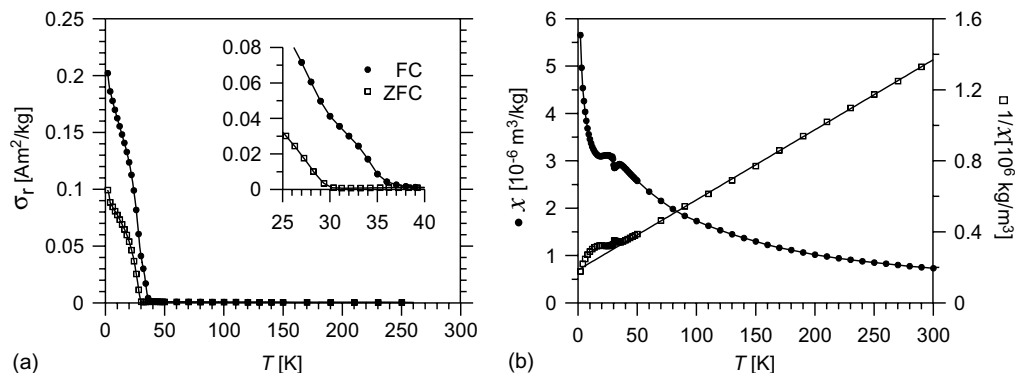


Fig. 5. Low-temperature magnetic characteristics of Norwegian Sea sediment (ODP Site 643, Leg 104, Sample 47-06-28, 446.88 m core depth). (a) Warming curves of 5 T remanence σ_r after cooling in zero field (open squares) and in a field of 5 T (solid dots). The insert clarifies the steep decay of remanence. For clarity only every fourth data point is represented by a symbol. (b) In-phase magnetic susceptibility χ versus temperature shows a plateau and subsequent drop around 29 K. The straight line marks a fit to the $1/\chi$ curve in the interval from 50 to 300 K plotted between axis limits.

scribed as large xenomorphic to hypidiomorphic crystals (Henrich, 1989). The ratio of FC to ZFC remanence is about 2:1, larger than the ratio for rhodochrosite, but less than for siderite (Fig. 5a). This intermediate value reasonably complies with the published Fe and Mn concentrations. FC remanence decays steeply from 2 up to 35 K virtually identical to the rhodochrosite reference. Yet, ZFC remanence vanishes entirely at 30 K. This 5 K offset between FC and ZFC curves results very likely from different unblocking temperatures possibly representing near-zero values of anisotropy constants. The higher coercive siderite component contributes very little to the ZFC curve. Therefore, we conclude that the 30 K decay corresponds to a marginally Fe-substituted rhodochrosite. In the FC curve, this predominant phase is responsible for the kink at 30 K. The higher unblocking temperature of 35 K is assigned to a manganosiderite, yet 2 K below the Néel point of the siderite reference.

Outside the critical range between 25 and 40 K, the $\chi(T)$ curve (Fig. 5b) of this sample coincides with the other sediment sample. After a steep initial decrease with rising temperature to 20 K, a little plateau develops, which drops off sharply at 29 K reflecting the presence of ferro-rhodochrosite. The following small maximum at 35 K indicates manganosiderite.

5. Discussion

The well-crystalline siderite and rhodochrosite reference samples reproduced thermal characteristics of FC and ZFC remanence as published by Housen et al. (1996). The respective ordering temperatures detected at 37 and 34 K (Table 2) agree with physics literature, but seem to represent upper limits for each mineral and decrease with impurities. The continuous solid solution series of $\text{Fe}^{2+}\text{-Mn}^{2+}$ carbonates commonly formed in

Table 2

Néel temperatures, peak values of in-phase susceptibility and remanence (FC, ZFC) at 2 and 4 K of natural siderite, rhodochrosite and vivianite well-crystalline samples

	Siderite FeCO ₃	Rhodochrosite MnCO ₃	Vivianite Fe ₃ [PO ₄] ₂ · 8H ₂ O
T_N [K]	37	34	12 (based on χ)
χ [10^{-6} m ³ /kg], peak value	5.24 (at 37 K)	151 (at 29 K)	6.62 (at 12 K)
σ_r [10^{-3} Am ² /kg], 5 T FC, 2 K	382	463	1.94
σ_r [10^{-3} Am ² /kg], 5 T ZFC, 2 K	51.5	327	1.61
σ_r (5 T FC): σ_r (5 T ZFC), 2 K	7.6:1	1.4:1	1.2:1
σ_r [10^{-3} Am ² /kg], 5 T FC, 4 K	381	455	1.28
σ_r [10^{-3} Am ² /kg], 5 T ZFC, 4 K	51.3	305	1.23
σ_r (5 T FC): σ_r (5 T ZFC), 4 K	7.4:1	1.5:1	1.04:1

marine sediments results in lower Néel temperatures down to 27 K and most likely beyond. Both spin-canted antiferromagnets acquire reasonable high-field remanences of 0.382 and 0.463 Am²/kg exceeding typical hematite values at room temperature (~ 0.2 Am²/kg). Non-stoichiometry appears to increase the remanence.

The normalized FC remanence curves of siderite and rhodochrosite are quite difficult to distinguish, whereas the ZFC remanence of siderite is more stable than that of rhodochrosite at temperatures below about 20 K (Fig. 6) contrasting with the findings of Housen et al. (1996). Depending on the respective mineralogical composition, it might not be easy to differentiate between siderite and rhodochrosite only by Néel temperatures or the shape of their ZFC and FC remanence curves. The most diagnostic difference is the ratio of FC and ZFC remanence at 2 K (Figs. 1a and 2a, Table 2).

Magnetic susceptibility may also be a useful diagnostic parameter, since the very low basal plane anisotropy of rhodochrosite can cause an abnormally high absolute χ which is much larger than that of siderite. The peak susceptibility for rhodochrosite observed here (1.51×10^{-4} m³/kg) reaches to one third of a typical magnetite value (5.7×10^{-4} m³/kg) at room temperature

(Heider et al., 1996). The extreme coercivity contrast between the easy basal plane and hard axis is clearly expressed by a near vertical segment in the hysteresis loops at low fields (Fig. 7). Deviations from the stoichiometric composition largely suppress spin waves and accordingly this hysteresis feature. The rotation into the hard direction appears to be temperature independent and proceeds almost linearly with the increasing field.

The hysteresis loops of siderite do not share this temperature independence nor the exotic near zero-field phenomenon of the rhodochrosite loops. However, these loops hold a remarkable feature of their own: The upward bending of the outer hysteresis branches at fields above ~ 5 T (Fig. 8a) is an indication of beginning metamagnetism. The available peak field of 7 T is sufficiently strong to initialize this forced transition from an antiferromagnetic to ferromagnetic state which only fully develops in the field range of 15–18 T (cf. Strykowski and Giordani, 1977). Completion of this first order magnetic phase transition would eventually be associated with a very large magnetic moment comparable to pure iron, providing an excellent, but experimentally expensive means of diagnosis.

The phenomenon of beginning metamagnetism at fields below 7 T is not restricted to siderite. Below the Néel temperature of 12 K, the hysteresis loops of vivianite are also upward bending (Fig. 8b). While the 7 K loop compares to siderite, the 2 K curve first bows down and then curls up at 7 T to near vertical further ascent. Low-field susceptibility and saturation magnetization of vivianite at 12 K exceed the respective values of siderite below its Néel temperature.

Also new to rock magnetic literature is the FC as well as ZFC remanence behavior of vivianite (Fig. 3a) differing distinctly from that of both other minerals.

However, a small residual field in the instrument (~ 0.15 mT) as suggested by the low remanence intensity, relatively high susceptibility and high resemblance of σ_r and χ curves below and above T_N interferes with the determination of T_N from remanence curves. The 12 K Néel point of vivianite is therefore best derived from magnetic susceptibility or induced magnetization curves. The two-stage rise of χ from 2 to 12 K (insert Fig. 3b)

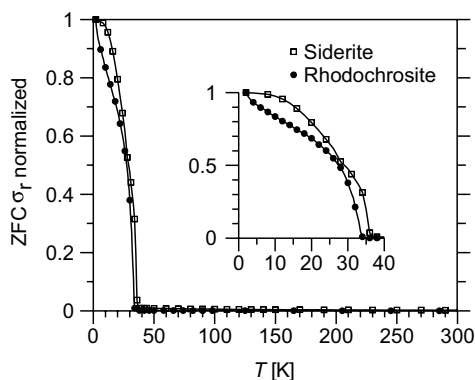


Fig. 6. Thermal decay of 5 T remanent magnetization σ_r (ZFC) of siderite and rhodochrosite normalized at 2 K. For clarity only every second (siderite) and eighth (rhodochrosite) data point is represented by a symbol. The insert shows the steep decay of remanence at the Néel temperature.

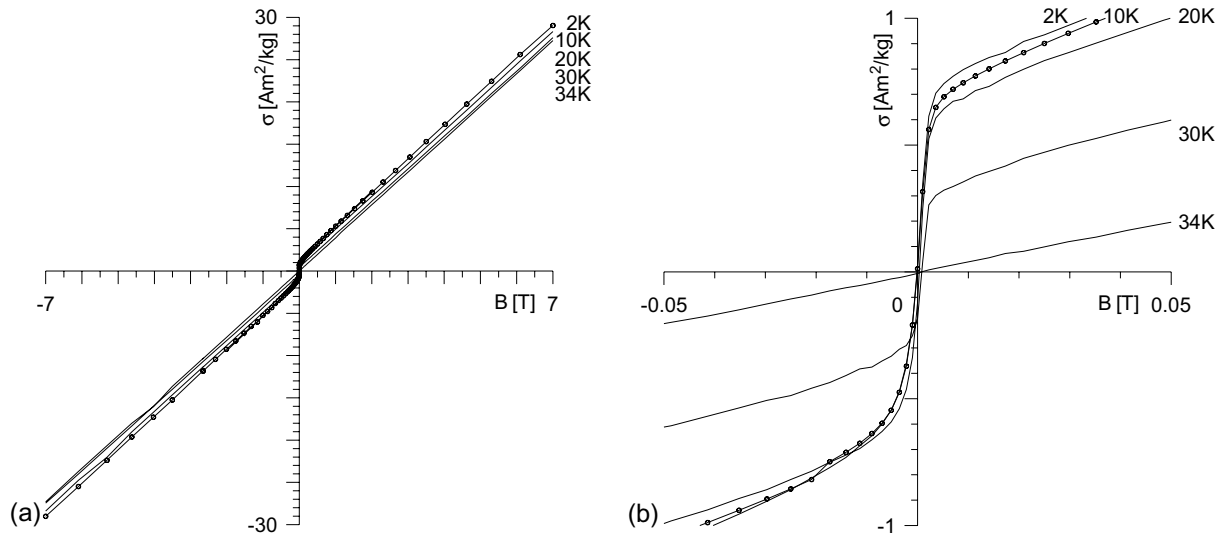


Fig. 7. (a) Upper branches of hysteresis loops of the well-crystalline rhodochrosite reference sample to peak magnetic fields of 7 T and (b) expanded field interval between -0.05 and $+0.05$ T. At each temperature, measurements were taken at the same evenly spaced intervals on a logarithmic scale. For clarity data point symbols are shown only for the 10 K hysteresis loop.

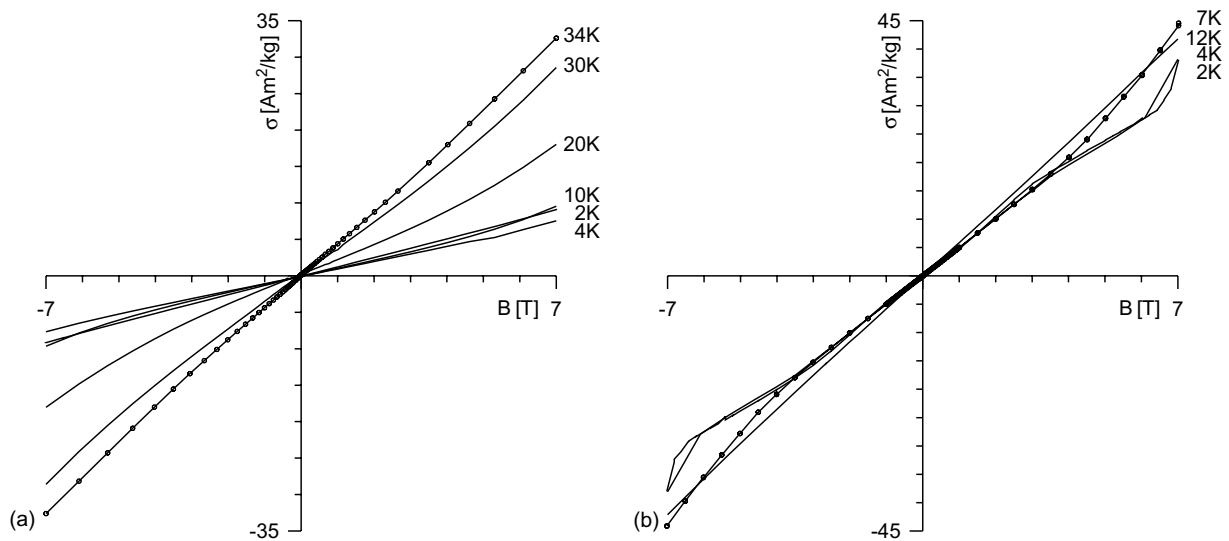


Fig. 8. Upper branches of hysteresis loops of the well-crystalline siderite (a) and vivianite (b) reference samples to peak magnetic field of 7 T. At each temperature, measurements were taken at the same evenly spaced intervals on a logarithmic scale. For clarity, data point symbols are shown only for the 34 K (siderite) and the 7 K (vivianite) hysteresis loop.

probably reflects successive magnetic ordering in planes and volume (Meijer et al., 1967).

6. Conclusions

Rhodochrosite, siderite, and vivianite show distinct magnetic low-temperature properties allowing a mutual discrimination as separate natural minerals. Besides temperature dependence of ZFC and FC remanence as well as of in-phase magnetic susceptibility, temperature dependent hysteresis loops are of diagnostic importance.

The detection limit of these low-temperature magnetic minerals in natural environments depends not so much on their own concentration, but rather on the presence of other strongly magnetic minerals exhibiting magnetic transitions in the temperature range below 40 K, for example the 34 K transition of pyrrhotite (Dekkers et al., 1989). Nevertheless, the low-temperature magnetic properties of marine sediment samples investigated here could be essentially explained by combining properties of their authigenic components rhodochrosite and manganosiderite. Therefore it should also be possible to identify these ferrous iron minerals in sediments of

unknown composition where they can precipitate only under certain anoxic conditions, far outside the stability field of Fe³⁺ bearing minerals.

Acknowledgements

We thank Rüdiger Henrich, Department of Geosciences, University of Bremen, for providing the marine sediment samples. We are also grateful to Heidi Hofer, Institute of Mineralogy, University of Frankfurt, Germany, for performing the electron microprobe analyses and to Horst D. Schulz and Henrik Hecht, Department of Geosciences, University of Bremen, for the chemical analyses (ICP-OES) of the mineral samples. We thank Subir K. Banerjee and Andrei Kosterov for their helpful reviews. TvD acknowledges support of the Netherlands Research Centre for Integrated Solid Earth Science (ISES) as a visiting research fellowship. The MPMS was granted by the Deutsche Forschungsgemeinschaft, grant no. BL 154/24-2. This study was partly funded by the Deutsche Forschungsgemeinschaft as part of the DFG-Research Center 'Ocean Margins' of the University of Bremen No. 0088.

References

- Bequerel, J., 1940. Le Magnétisme. Institut International de Coopération Intellectuelle Paris, CNRS.
- Borovik-Romanov, A.S., 1959. Investigations of weak ferromagnetism in the MnCO₃ single crystal. *Sov. Phys. JETP* 36, 539–549.
- Burns, S., 1997. Early diagenesis in Amazon Fan sediments. In: Flood, R.D., Piper, D.J.W., Klaus, A., Peterson, L.C. (Eds.), *Proc. ODP., Sci. Results*, vol. 155, pp. 497–504.
- Canfield, D.E., Raiswell, R., Bottrell, S., 1992. The reactivity of sedimentary iron minerals toward sulfide. *Am. J. Sci.* 292, 659–683.
- Chow, N., Morad, S., Al-Aasm, I.S., 2000. Origin of authigenic Mn–Fe carbonates and pore-water evolution in marine sediments: Evidence from Cenozoic strata of the Arctic Ocean and Norwegian–Greenland Sea (ODP Leg 151). *J. Sediment. Res.* 70, 682–699.
- Deike, R.G., Granina, L., Callender, E., McGee, J.J., 1997. Formation of ferric iron crusts in Quaternary sediments of Lake Baikal, Russia, and implications for paleoclimate. *Mar. Geol.* 139, 21–46.
- Dekkers, M.J., Mattéi, J.-L., Fillion, G., Rochette, P., 1989. Grain-size dependence of the magnetic behavior of pyrrhotite during its low-temperature transition at 34 K. *Geophys. Res. Lett.* 16, 855–858.
- Dekkers, M.J., Passier, H.F., Schoonen, M.A.A., 2000. Magnetic properties of hydrothermally synthesized greigite (Fe₃S₄)-II. High- and low-temperature characteristics. *Geophys. J. Int.* 141, 809–819.
- Dudko, K.L., Eremenko, V.V., Fridman, V.M., 1975. Investigation of the transition of FeCO₃ from the antiferromagnetic to the paramagnetic state under the influence of a strong magnetic field. *Sov. Phys. JETP* 41, 326–332.
- Ellwood, B.B., Burkart, B., Long, G.J., Buhl, M.L., 1986. Anomalous magnetic properties in rocks containing the mineral siderite: paleomagnetic implications. *J. Geophys. Res.* 91, 12779–12790.
- Ellwood, B.B., Burkart, B., Raheshwar, K., Darwin, R.L., Neeley, R.A., McCall, A.B., Long, G.J., Buhl, M.L., Hickcox, C.W., 1989. Are the iron carbonate minerals, ankerite and ferroan dolomite, like siderite, important in paleomagnetism? *J. Geophys. Res.* 94, 7321–7331.
- Forst, H., Love, N.D., McElearney, J., 1965. Specific heat of Fe₃(PO₄)₂·8H₂O. *Phys. Rev.* 129, A1256–A1248.
- Forsyth, J.B., Johnson, C.E., Wilkinson, C., 1970. The magnetic structure of vivianite, Fe₃(PO₄)₂·8·H₂O. *J. Phys. C: Solid State Phys.* 3, 1127–1139.
- Frederichs, T., Bleil, U., Däumler, K., von Dobeneck, T., Schmidt, A., 1999. The magnetic view on the marine paleoenvironment: parameters, techniques and potentials of rockmagnetic studies as a key to paleoclimatic and paleoceanographic changes. In: Fischer, G., Wefer, G. (Eds.), *Use of Proxies in Paleoclimatology: Examples from the South Atlantic*. Springer, Berlin, pp. 575–599.
- Glasby, G.P., Schultz, H.D., 1999. *E_H*, pH diagrams for Mn, Fe, Co, Ni, Cu and As under seawater conditions: applications of two new types of *E_H*, pH diagrams to the study of specific problems in marine geochemistry. *Aquatic Geochem.* 5, 227–248.
- Grodzicki, M., Amthauer, G., 2000. Electronic and magnetic structure of vivianite: cluster molecular orbital calculations. *Phys. Chem. Miner.* 27, 694–702.
- Haese, R.R., Wallmann, K., Dahmke, A., Kretzmann, U., Müller, P.J., Schulz, H.D., 1997. Iron species determination to investigate early diagenetic reactivity in marine sediments. *Geochim. Cosmochim. Acta* 61, 63–72.
- Heider, F., Zitzelsberger, A., Fabian, K., 1996. Magnetic susceptibility and remanent coercive force in grown magnetite crystals from 0.1 μm to 6 mm. *Phys. Earth Planet. Int.* 93, 239–256.
- Henrich, R., 1989. Diagenetic environments of authigenic carbonates and opal-ct crystallization in lower Miocene to upper Oligocene deposits of the Norwegian Sea (ODP Site 643, Leg 104). In: Eldholm, O., Thiede, J., Taylor, E. et al. (Eds.), *Proc. ODP., Sci. Results*, vol. 104, pp. 233–247.
- Hirt, A.M., Lanci, L., Dobson, J., Weidler, P., Gehring, A.U., 2002. Low-temperature magnetic properties of lepidocrocite. *J. Geophys. Res.* 107 (B1), doi:10.1029/2001JB000242.
- Housen, B.A., Banerjee, S.K., Moskowicz, B.M., 1996. Low-temperature magnetic properties of siderite and magnetite in marine sediments. *Geophys. Res. Lett.* 23, 2843–2846.
- Hurlbut Jr., C.S., 1971. *Dana's Manual of Mineralogy*, Eighteenth ed. John Wiley & Sons, New York.
- Hus, J.J., 1990. The magnetic properties of siderite concretion and the CRM of their oxidation products. *Phys. Earth Planet. Inter.* 63, 41–57.
- Jacobs, I.S., 1963. Metamagnetism of siderite (FeCO₃). *J. Appl. Phys.* 34, 1106–1107.
- Kleinberg, R., 1969. Magnetic structure of vivianite Fe₃(PO₄)₂·8H₂O. *J. Chem. Phys.* 51, 2279–2280.
- Konhauser, K.O., 1998. Diversity of bacterial iron mineralization. *Earth Sci. Rev.* 43, 91–121.
- Manning, P.G., Prepas, E.E., Serediak, M.S., 1999. Pyrite and vivianite intervals in bottom sediments of eutrophic baptiste lake, Alberta, Canada. *Can. Mineral.* 37, 593–601.
- Maher, B.A., Thompson, R. (Eds.), 1999. *Quaternary Climates, Environments and Magnetism*. Cambridge University Press, Cambridge.
- Mays, J.M., 1957. Second-nearest-neighbor nuclear magnetic resonance shifts in iron group phosphates. *Phys. Rev.* 108, 1090–1091.
- Meijer, H.C., van den Handel, J., Frikkee, E., 1967. Magnetic behavior of vivianite, Fe₃(PO₄)₂·8H₂O. *Physica* 34, 475–483.
- Morad, S., Al-Aasm, I.S., 1997. Conditions of rhodochrosite-nodule formation in Neogene–Pleistocene deep-sea sediments: Evidence from O, C, and Sr isotopes. *Sediment. Geol.* 114, 295–304.
- Nealson, K.H., Saffarini, D., 1994. Iron and manganese in anaerobic respiration: environmental significance, physiology, and regulation. *Ann. Rev. Microbiol.* 48, 311–343.
- Neumann, T., Heiser, U., Leosson, M.A., Kersten, M., 2002. Early diagenetic processes during Mn-carbonate formation: evidence from the isotopic composition of authigenic Ca-rhodochrosites of the Baltic Sea. *Geochim. Cosmochim. Acta* 66, 867–879.

- Ozhogin, V.I., 1963. The antiferromagnets CoCO_3 , CoF_2 , and FeCO_3 in strong fields. *J. Exp. Theor. Phys. (USSR)* 45, 1687–1690.
- Pan, Y., Zhu, R., Banerjee, S.K., Gill, J., Williams, Q., 2000. Rock magnetic properties related to thermal treatment of siderite: behavior and interpretation. *J. Geophys. Res.* 105, 783–794.
- Peters, C., 1995. Unraveling magnetic mixtures in sediments, soils and rocks. Ph.D. thesis, University of Edinburgh, Department of Geology and Geophysics, p. 206.
- Peters, C., Dekkers, M.J., 2003. Room temperature magnetic parameters as a function of concentration, grain size and mineralogy. *Phys. Chem. Earth* 28, 659–667.
- Peters, C., Thompson, R., 1999. Superparamagnetic enhancement, superparamagnetism, and archaeological soils. *Geoarchaeology* 14, 401–413.
- Robie, R.A., Haselton Jr., H.T., Hemingway, B.S., 1984. Heat capacities and entropies of rhodochrosite (MnCO_3) and siderite (FeCO_3) between 5 and 600 K. *Am. Mineral.* 69, 349–357.
- Rodriguez, N.M., Paull, C.K., Borowski, W.S., 2000. Zonation of authigenic carbonates within gas hydrate-bearing sedimentary sections on the Blake Ridge, offshore southeastern North America. In: Paull, C.K., Matsumoto, R., Wallace, P.J., Dillon, W.P. (Eds.), *Proc. ODP., Sci. Results*, vol. 164, pp. 301–312.
- Schulz, H.D., Dahmke, A., Schinzel, U., Wallmann, K., Zabel, M., 1994. Early diagenetic processes, fluxes and reaction rates in sediments of the South Atlantic. *Geochim. Cosmochim. Acta* 58, 2041–2060.
- Senftle, F.E., Thorpe, A.N., Briggs, C., Alexander, C., Minkin, J., Griscom, D.L., 1975. The Néel transition and magnetic properties of terrestrial, synthetic, and lunar ilmenites. *Earth Planet. Sci. Lett.* 26, 377–386.
- Sifeddine, A., Martin, L., Ture, B., Volkmer-Ribeiro, C., Soubiès, F., Cordeiro, R.C., Suguio, K., 2001. Variations of the Amazonian rainforest environment: A sedimentological record covering 30,000 years. *Paleoeco., Paleoclim., Paleoecol.* 168, 221–235.
- Stevens, L.R., Ito, E., Olson, D.E.L., 2000. Relationship of Mn-carbonates in varved lake sediments to catchment vegetation in Big Watab Lake, MN, USA. *J. Paleolim.* 24, 199–211.
- Stryjewski, E., Giordani, N., 1977. *Metamagnet.* *Adv. Phys.* 26, 487–650.
- Vriend, S.P., Dekkers, M.J., Janssen, M.A., Commandeur, J., 1991. Well sediments: A medium for geochemical prospecting, an example from the Nisa region, Portugal. In: Rose, A.W., Taufen, P.M. (Eds.), *Geochemical exploration 1989.* *J. Geochem.* 41, 151–167.
- Walker, D., Owen, J.A.K., 1999. The characteristics and source of laminated mud at Lake Barrine, Northeast Australia. *Quat. Sci. Rev.* 18, 1597–1624.
- Worm, H.U., Jackson, M., 1999. The superparamagnetism of Yucca Mountain tuff. *J. Geophys. Res.* 104, 25415–25425.
- Zabel, M., Schneider, R.R., Wagner, Z., Adegbie, A., de Vries, U., Kolonic, S., 2001. Late Quaternary climate changes in central Africa as inferred from terrigenous input to the Niger Fan. *Quat. Res.* 56, 207–217.
- Zergenyi, R.S., Hirt, A.M., Zimmermann, S., Dobson, J.P., Lowrie, W., 2000. Low-temperature magnetic behavior of ferrihydrite. *J. Geophys. Res.* 105, 8297–8303.